crystals

MDPI

Article

Interfacial Microstructure and Mechanical Properties of Titanium/Sapphire Joints Brazed with AuSn20 Filler Metal

Yi Zhou [1], Hong Bian [1,2,*], Xiaoguo Song [1,2], Yuzhen Lei [1,2], Mingjun Sun [1], Weimin Long [3], Sujuan Zhong [4] and Lianhui Jia [5]

1 State Key Laboratory of Advanced Welding and Joining, Harbin Institute of Technology, Harbin 150001, China
2 Shandong Institute of Shipbuilding Technology, Weihai 264209, China
3 China Machinery Intelligent Equipment Innovation Research Institute (Ningbo) Co., Ltd., Ningbo 315700, China
4 State Key Laboratory of Advanced Brazing Filler Metals and Technology, Zhengzhou Research Institute of Mechanical Engineering Co., Ltd., Zhengzhou 450001, China
5 China Railway Engineering Equipment Co., Ltd., Zhengzhou 450016, China
* Correspondence: bianhong@hit.edu.cn

Abstract: In this study, C-plane (0001) sapphire was successfully brazed to titanium using AuSn20 filler metal, following metallization on the surface of the sapphire with Sn-3Ti (wt.%). At 1000 °C, Sn-3Ti had good wettability on the surface of the sapphire, with the lowest equilibrium contact angle of 57°. The reaction phases in the joints were identified, and the typical interfacial microstructure of the brazed joint brazed at 550 °C for 30 min was titanium substrate/Au-Sn-Ti layer/Ti_6Sn_5 + $AuSn_2$ + $AuSn_4$ + massive Au-Sn-Ti/TiO phase/sapphire. The shear test was utilized to evaluate the bonding strength of the titanium/sapphire joints. The highest shear strength reached 18.7 MPa when brazed at 550 °C for 35 min. The crack was initiated at the sapphire/brazing seam interface and propagated into the Au-Sn-Ti reaction layer.

Keywords: brazing; titanium; sapphire; metallization; microstructure; mechanical properties

check for updates

Citation: Zhou, Y.; Bian, H.; Song, X.; Lei, Y.; Sun, M.; Long, W.; Zhong, S.; Jia, L. Interfacial Microstructure and Mechanical Properties of Titanium/Sapphire Joints Brazed with AuSn20 Filler Metal. *Crystals* **2022**, *12*, 1687. https://doi.org/10.3390/cryst12121687

Academic Editors: Dawei Zhao, Ricardo Branco, Fábio Fernandes and Bappa Acherjee

Received: 22 October 2022
Accepted: 19 November 2022
Published: 22 November 2022

1. Introduction

Sapphire exhibits excellent properties, such as good optical performance, high stiffness, superior thermal stability, good biocompatibility, and good corrosion resistance [1]. It has been used in medical and chemical equipment and the aerospace industries [2–6]. Titanium possesses significant potential for the aerospace area, medical equipment, and other industrial fields [7–9] due to its perfect performance in such areas as oxidation resistance and its outstanding mechanical properties. The biocompatible metal–ceramic joints used for biomedical applications such as implantable pacemakers and retinal implants have received remarkable attention [10]. In addition, some implantable devices, such as retinal implants, work by optical signals. In order to ensure the good biocompatibility and optical performance of the components, it is of great significance to investigate the joining behavior between sapphire and titanium.

Currently, various joining techniques are being applied to achieve the reliable joining of ceramics to themselves or metals (alloys) [11]. Brazing, with good repeatability and relatively small thermal effect, is the main method used in the field of dissimilar material bonding [12–14]. However, the different types of chemical bonds cause problems such as poor wettability and poor metallurgical bonding. Currently, one of effective solutions is to metalize the ceramics by coating the surface with a metallization layer [15–19], and the proper choice of material for metallizing is pivotal to realize metallurgical bonding at the interface of the ceramics. Sn-based filler metal was widely used to provide a reliable connection for ceramics and metal at the low temperatures. Song et al. [20] studied the brazeability of Sn0.3Ag0.7Cu-3 wt.% Ti on SiC ceramics, and the average shear strength

of the SiC joints reached 15.6 MPa. Kang et al. [21] studied the wettability of SnAgCu-Ti alloys on alumina. The minimum contact angle of 14.4 deg was reached when the droplet contained 3 wt.% Ti. Alumina/alumina joints without pores were obtained and the maximum strength of 28.6 MPa was achieved using SnAgCu-2Ti. However, the heavy use of Ag and Cu can be harmful to the human body. Fu et al. [22] studied the interfacial behavior of Sn-Ti alloys on zirconia. When 4Ti (at.%) was added, the lowest contact angle of 22 deg was obtained, owing to the replacement of Ti_2O_3 by the $Ti_{11.31}Sn_3O_{10}$ layer at the interface. Considering the wettability and biocompatibility, Sn-3Ti (wt.%) was used for the metallization on the surface of sapphire.

Another difficulty is the large residual stress due to high temperature and the difference in the coefficients of thermal expansion between ceramics and metal [23–26]. Thus, a low brazing temperature has vital importance. Adding low-melting-point elements (In, Sn, Ga, Bi) [27,28] to the solder alloy to reduce the connection temperature can be used to relieve residual stress. AuSn20 (wt.%) eutectic filler is widely used in the electronic packaging and medical device industry due to its good biocompatibility, low melting temperature (278 °C), high thermal conductivity, excellent corrosion resistance, and many other advantages [29–35]. Therefore, AuSn20 solder was used to braze to ensure the mechanical property and biocompatibility of the brazed joints.

Firstly, in this study, the wettability of the Sn-3Ti alloy on the C-plane sapphire surface was studied. The variation of contact angles in the continuous-heating process was studied to better instruct the following joining processes, and the cross-sectional microstructure of Sn-3Ti/sapphire system was characterized. Then, the surface of the C-plane sapphire was metallized with Sn-3Ti at 1000 °C for 30 min, and AuSn20 solder was used to braze the joint between the titanium and the C-plane sapphire. The interfacial microstructure and mechanical properties of the joints were investigated in detail.

2. Materials and Experimental Procedure

Commercial sapphire, with the dimensions of 5 × 5 × 5 mm^3 and 10 × 10 × 1 mm^3, was supplied by Guizhou Haotian Optoelectronics Technology Co., Ltd., Guizhou, China. The dimensions of the pure titanium used herein was 5 × 10 × 5 mm^3. The Sn-3Ti was arc-melted and remelted more than three times, and the microstructure of the Sn-3Ti alloy is shown in Figure 1a. It revealed that the Ti_6Sn_5 phase was distributed homogeneously in the β-Sn matrix. AuSn20 alloy (Bolin electronic packaging materials Co., Ltd., Guangdong, China) was used as a brazing filler metal, with the dimensions of 5 mm × 5 mm × 50 μm. Figure 1b shows that the AuSn20 brazing alloy mainly consisted of a Au_5Sn phase and a AuSn phase.

Wetting experiments were performed using the sessile drop method. The Sn-3Ti alloy (0.25 g) was pre-placed on the surface of the sapphire (10 × 10 × 1 mm^3) by the method described in Refs. [36,37]. A digital camera was used to record the outline of the droplet in the wetting process at the speed of 1 frame/6s. Subsequently, the Sn-3Ti foil (150 μm) was placed on the surface (with an area of 5 × 5 mm^2) of the sapphire to realize the metallization process, and then, the brazing experiments were performed. To ensure the optimum planarity and an intimate contact, each specimen was polished using silicon carbide paper with the grit size of 800# and was ultrasonically cleaned in acetone before brazing. The assembly diagram is shown in Figure 1c,d. The experimental parameters of wetting, metallization, and brazing are listed in Table 1.

Table 1. Experimental parameters.

Process	Temperature	Time	Vacuum
Wetting	1050 °C	-	3.0×10^{-3} Pa
Metallization	1000 °C	10 min	
Brazing	450 °C to 650 °C	20 min to 35 min	

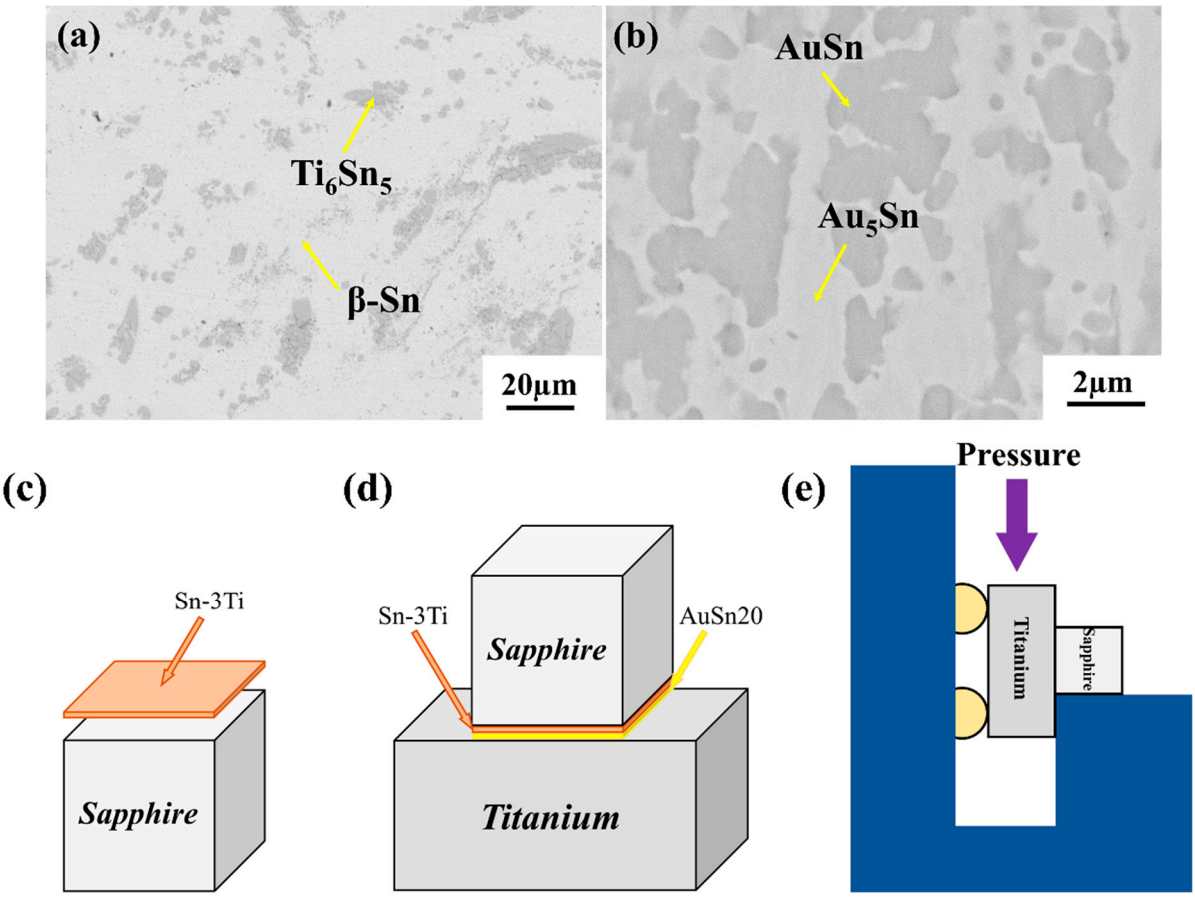

Figure 1. Microstructure of (**a**) Sn-3Ti and (**b**) AuSn20 and schematic diagram of (**c**) surface metallization test, (**d**) brazing assembly, and (**e**) shear test.

Cross-sections of the brazing joints were characterized by scanning electron microscopy (SEM) equipped with an energy dispersive X-ray spectroscopy (EDS). The reaction phase formed on the sapphire side was investigated by transmission electron microscope (TEM). The joining properties of the brazed joints at room temperature were characterized using a universal testing machine (INSTRON, 5967) with a constant speed of 0.5 mm/min. The diagram of the shear test is shown in Figure 1e. At least five samples were tested for each experimental parameter. The fracture of the joints was characterized by SEM.

3. Results and Discussion

3.1. The Wetting Phenomena of Sn-3Ti/Sapphire

Figure 2 shows the variation of contact angles of the Sn-3Ti droplet on the surface of the sapphire with the increasing temperature. The wetting angle changes could be parted into three stages: (I) Sn-3Ti melted completely until 700 °C with the contact angle of 107°; (II) at 700 °C < T < 1000 °C, the contact angle decreased and kept a fast wetting speed; and (III) at T > 1000 °C, the contact angles decreased slowly with a final contact angle of 57°. Figure 3a,b show the cross-sectional microstructure of the Sn-3Ti/sapphire system. The corresponding EDS analysis (Table 2) revealed that the matrix was β-Sn (marked as A), and the dark phases in the droplets were Ti_6Sn_5 (marked as B).

Table 2. EDS chemical analysis of the regions marked in Figure 3b (at.%).

Spot	Sn	Ti	Possible Phases
A	100.00	0	β-Sn
B	41.22	58.78	Ti_6Sn_5

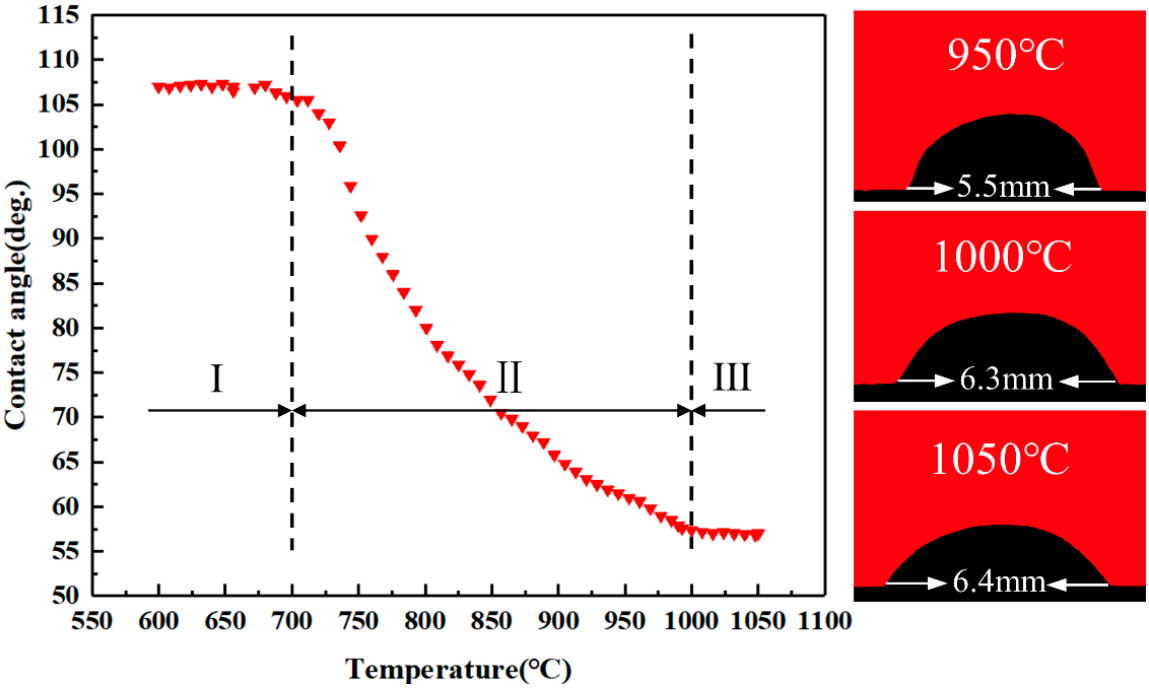

Figure 2. Variation of contact angle for Sn-3Ti/sapphire system at different wetting temperatures and profiles of drops at 950 °C, 1000 °C, and 1050 °C.

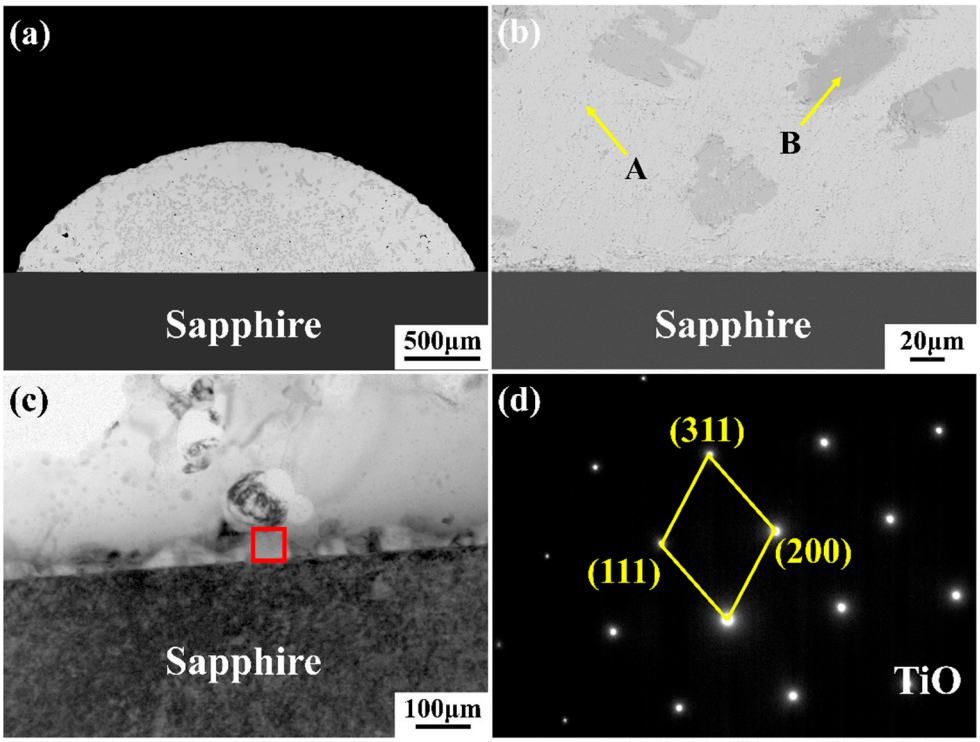

Figure 3. (**a**) Interfacial microstructure of Sn-3Ti/sapphire system; (**b**) high-magnification details of (**a**); (**c**) TEM micrographs of TiO grain from the interface; and (**d**) the SAED patterns corresponding to the zone indicated in (**c**).

To verify the reaction phase on the sapphire side, TEM characterization was conducted. Figure 3c shows that a new phase was formed at the interface between the sapphire and the droplet. The corresponding selected area electron diffraction (SAED) certified that the

phase was TiO, as shown in Figure 3d. TiO could serve as a "bridge" to join the filler metal to the ceramic substrate strongly, which coincided with the results reported in Refs. [38–45].

3.2. Typical Interfacial Microstructure of the Titanium/AuSn20/Sn-3Ti/Sapphire Joint

Figure 4 displays the microstructure and the energy-dispersive spectrometer compositional maps of the titanium/AuSn20/Sn-3Ti/sapphire joint brazed at 550 °C for 30 min. In Figure 4a, a sound joint without any crack or void can be seen, indicating a close contact between the titanium and the sapphire. According to Figure 4c–e, the elements Au, Sn, and Ti are mainly distributed in the Sn-Ti, Au-Sn, and Au-Sn-Ti intermetallic compounds. As shown in Figure 4f,g, the element O and Al were mainly distributed in the sapphire, and the enrichment of O was found at the interface of the brazing seam/sapphire.

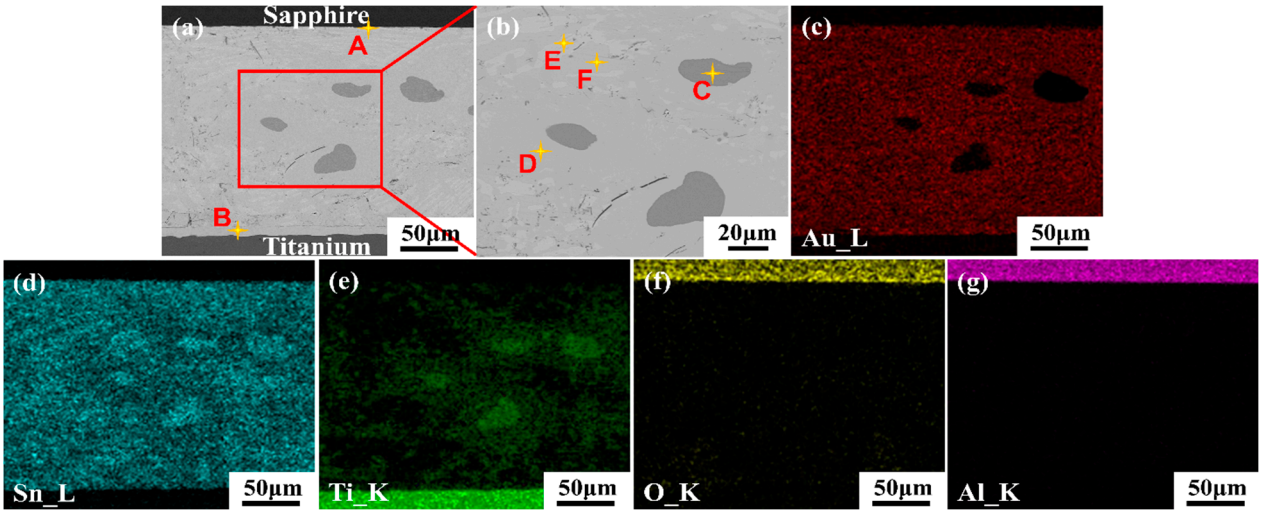

Figure 4. Analyses of the titanium/AuSn20/Sn-3Ti/sapphire joint brazed at 550 °C for 30 min: (**a**) typical interfacial microstructure; (**b**) the high-magnification image of the brazing seam; and (**c**–**g**) element map distributions of Au, Sn, Ti, O, and Al.

To investigate the microstructure characteristics of the titanium/AuSn20/Sn-3Ti/sapphire joint in detail, all the phases were marked by A–F, and the corresponding EDS results for the typical joint are listed in Table 3. Combined with the chemical compositions in Table 3, the dark phase marked by A was confirmed as TiO. Both the B and the D phases were Au-Sn-Ti. The regions of C, E, and F were Ti_6Sn_5, $AuSn_2$, and $AuSn_4$, respectively. To sum up, the final interfacial microstructure of the titanium/AuSn20/Sn-3Ti/sapphire joint brazed at 550 °C for 30 min was titanium substrate/Au-Sn-Ti layer/Ti_6Sn_5 + $AuSn_2$ + $AuSn_4$ + massive Au-Sn-Ti/TiO phase/sapphire.

Table 3. EDS chemical analysis of the regions marked in Figure 4a,b (at.%).

Spot	Au	Sn	Ti	Al	O	Possible Phases
A	2.00	1.40	40.30	1.60	54.70	TiO
B	25.11	40.41	29.11	0	0	Au-Sn-Ti
C	0	40.58	56.81	0	0	Ti_6Sn_5
D	27.33	42.04	30.63	0	0	Au-Sn-Ti
E	33.53	58.29	0.30	0.30	7.58	$AuSn_2$
F	23.10	76.90	0	0	0	$AuSn_4$

3.3. Effects of Processing Parameters on the Microstructure of the Titanium/AuSn20/Sn-3Ti/Sapphire Joint

Figures 4a and 5 show the microstructure evolution of the joint brazed at 450 °C, 500 °C, 550 °C, 600 °C, and 650 °C for 30 min. At a low brazing temperature (450 °C), as

shown in Figure 5a, a discontinuous Au-Sn-Ti reaction layer was formed. Subsequently, the thickness of the Au-Sn-Ti adjacent to the titanium increased as the brazing temperature increased. This phenomenon could be interpreted by the accelerated dissolution of Ti atoms into the interlayer. It is worth noting that the morphology of the brazing seam also underwent significant changes. With increasing temperature, the volumes of the Ti_6Sn_5 phase and the $AuSn_2$ phase became gradually smaller. With the further increasing of the brazing temperature to 650 °C, the Ti_6Sn_5 phase disappeared, and the entire region was almost occupied with the Au-Sn-Ti phase and the $AuSn_4$ phase, as shown in Figure 5d. Microcracks were induced on the sapphire side, which indicated that the residual stress of the joints increased due to high temperature.

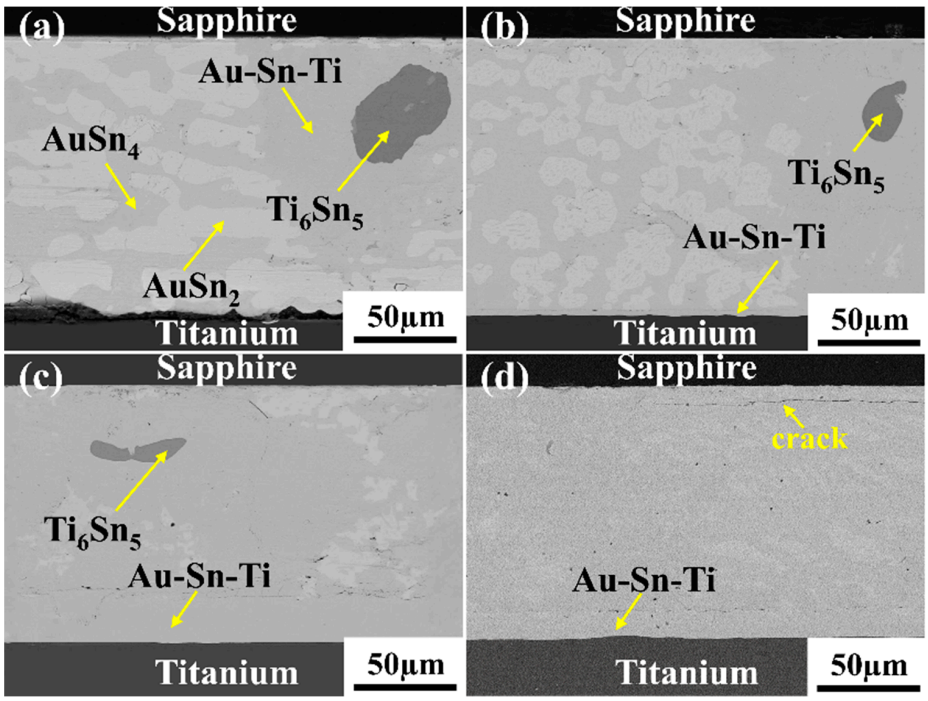

Figure 5. Interfacial microstructure of the titanium/AuSn20/Sn-3Ti/sapphire joints brazed at (**a**) 450 °C, (**b**) 500 °C, (**c**) 600 °C, and (**d**) 650 °C.

Figures 4a and 6 show the microstructure of the joints brazed at 550 °C for different holding times. With the extension of the holding time, the inter-diffusion of atoms between the brazing filler metal and the base metal was enhanced. The volumes of the Ti_6Sn_5 phase and the $AuSn_2$ phase became gradually smaller. Additionally, the Au-Sn-Ti layer next to the sapphire did not change significantly.

To conclude, the microstructure of the titanium/AuSn20/Sn-3Ti/sapphire joints could be controlled by the dissolution and diffusion of the active atoms at different brazing temperatures. According to the observation of the cross-sectional parts above, a schematic was established to show the forming process. According to the Sn-Ti binary phase diagram [36], the melting point of Ti_6Sn_5 was 1490 °C and the melting point of β-Sn was 231.9 °C. When heated to 231.9 °C and 278 °C, the β-Sn in the metallization layer and the AuSn20 filler metal commenced to melt and liquid formed, respectively. The Ti_6Sn_5 phase and the TiO phase which formed during the metallization process consequently remained solid, as illustrated in Figure 7a. Subsequently, an amount of Ti from the titanium substrate diffused into the molten AuSn20 filler metal caused by the concentration gradient and reacted with Au and Sn to form a Au-Sn-Ti reaction layer when brazed at 550 °C. Meanwhile, the Au diffused into the metallization layer and reacted with the Ti_6Sn_5 to form Au-Sn-Ti. During the cooling process, some of the $AuSn_4$ and $AuSn_2$ phases precipitated from the liquid phase. Eventually, the titanium/AuSn20/Sn-3Ti/sapphire joints were obtained, as shown

in Figure 7b. When the brazing temperature increased, the Ti_6Sn_5 phase disappeared, and the volume of the $AuSn_2$ became small due to the adequate reaction between the Ti_6Sn_5 and the $AuSn_2$. Correspondingly, the brazing seam was almost occupied with Au-Sn-Ti and $AuSn_4$. The thickness of Au-Sn-Ti layer adjacent to the titanium substrate increased, as shown in Figure 7c.

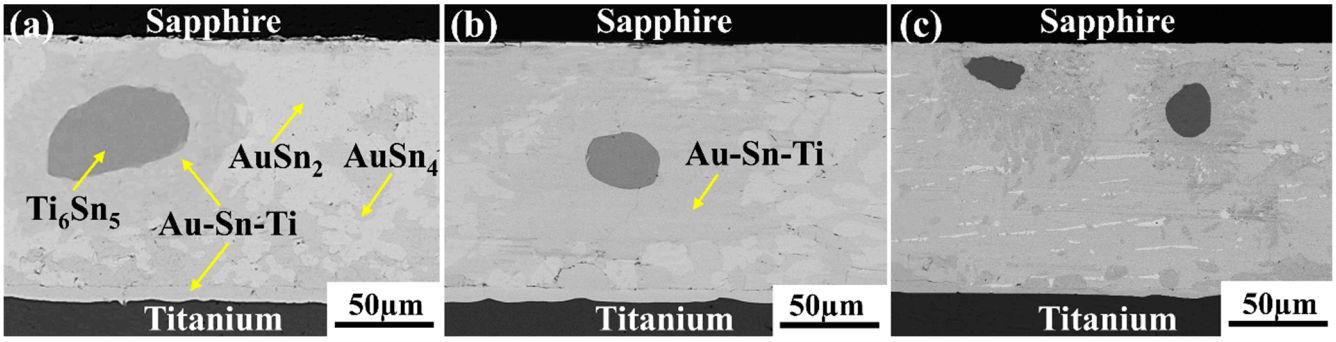

Figure 6. Interfacial microstructure of the titanium/AuSn20/Sn-3Ti/sapphire joints brazed at 550 °C for (**a**) 20 min, (**b**) 25 min, and (**c**) 35 min.

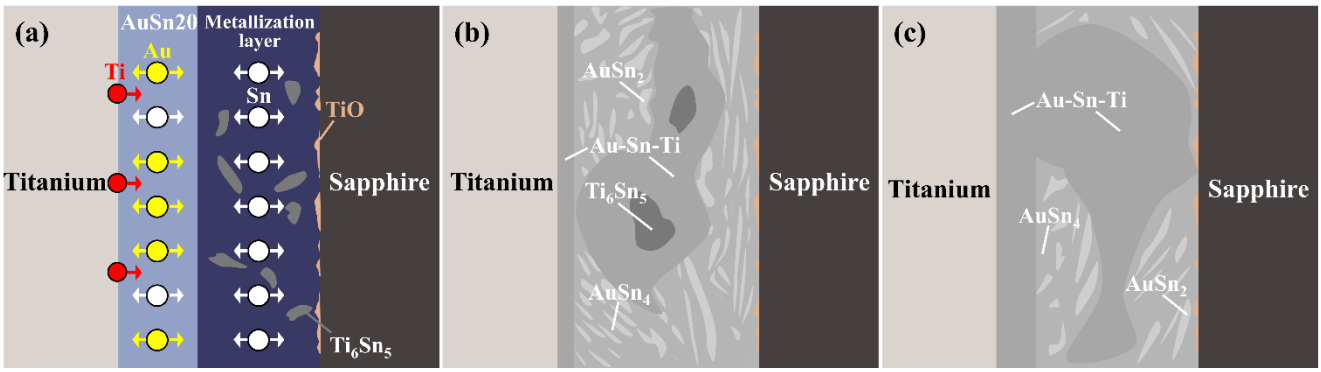

Figure 7. Schematic diagram of the microstructure evolution of titanium/AuSn20/Sn-3Ti/sapphire joint: (**a**) atomic diffusion; (**b**) formation of reaction products at 550 °C; and (**c**) interfacial structure of the brazing seam at 650 °C.

3.4. Mechanical Properties and Fracture Morphology of the Titanium/AuSn20/Sn-3Ti/Sapphire Joint

Figure 8a illustrates that the shear strength of the titanium/AuSn20/Sn-3Ti/sapphire joints increased from 4.0 MPa to 12.9 MPa, with the brazing temperature increasing from 450 °C to 550 °C and then dropping to 10.2 MPa when brazed at 650 °C. The obtained maximum strength was 12.9 MPa at 550 °C, which was about three times that of the joints brazed at 450 °C. Under a different holding time, the maximum shear strength reached 18.7 MPa when holding for 35 min, as shown in Figure 8b.

In order to further analyze the causes of the different failure modes, the fracture cross-section of the joints was observed by SEM and EDS, and the fracture modes were summarized, as shown in Figure 9. As the metallurgical bonding of the ceramic side was achieved through the formation of the TiO phase in the metallization stage, the brazing temperature affected the fracture of the joints mainly by the phase formation in the other areas of the brazing seam and the residual stress in the joint. When brazed at 450 °C, a straight crack path was observed (Figure 9a,b). The joints failed on the titanium side, owing to the discontinuous Au-Sn-Ti reaction phase adjacent to the titanium, as depicted in Figure 5a. When the brazing temperature rose to 550 °C, the residual stress in the sapphire accumulated gradually; so, the crack was initiated at the sapphire and propagated along the brazing seam during the shear test (Figure 9d). Meanwhile, the Au-Sn-Ti reaction layer

with a certain thickness was formed on the titanium side so that the crack propagated into this brittle reactive layer (Figure 9e). When brazed at 650 °C, the joints fractured along the brazing seam/sapphire interface (Figure 9g,h). The high modulus of elasticity and hardness of the sapphire made it show a low plastic deformation ability, which resulted in large residual stress in the joint.

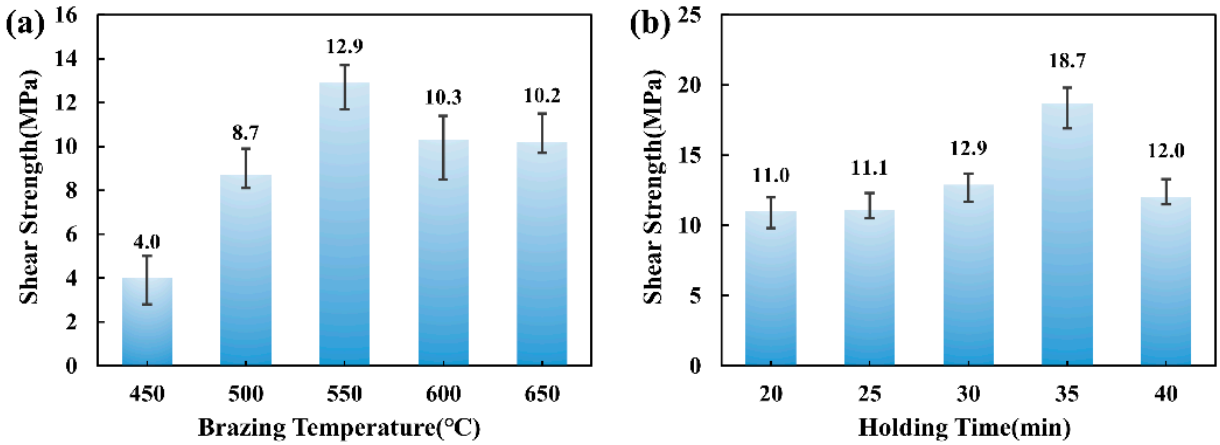

Figure 8. Shear strength of the titanium/AuSn20/Sn-3Ti/sapphire joints: (**a**) different brazing temperature and (**b**) different holding time.

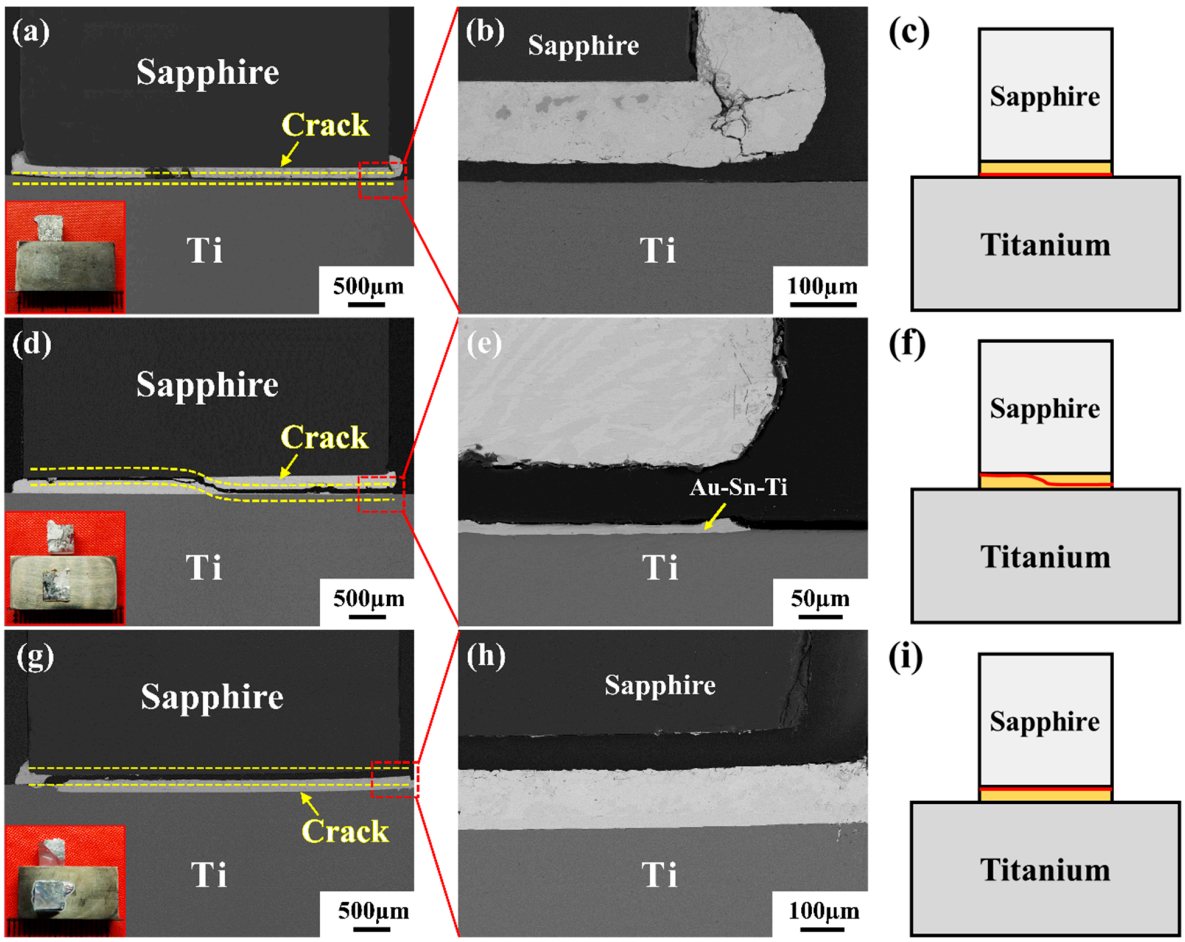

Figure 9. Fracture cross-section of the joints at (**a**,**b**) 450 °C, (**d**,**e**) 550 °C, and (**g**,**h**) 650 °C and diagram of fracture paths at (**c**) 450 °C, (**f**) 550 °C, and (**i**) 650 °C.

4. Conclusions

Reliable brazing of the titanium and sapphire was achieved by using AuSn20 under the premise of pre-metallization on the surface of the sapphire. The wettability of Sn-3Ti on sapphire was studied. The microstructure and mechanical properties of the brazed joints were investigated. The details of the conclusion are as follows:

1. The lowest equilibrium contact angle of Sn-3Ti on the sapphire substrate in the wetting experiment was 57°. In the Sn-3Ti/sapphire system, the Ti6Sn5 phase was formed in the solidified melt, which distributed in the Sn matrix. Meanwhile, TiO was formed at the interface between the sapphire and the droplet.
2. The typical interfacial microstructure of the titanium/AuSn20/Sn-3Ti/sapphire brazed joints was titanium substrate/Au-Sn-Ti layer/Ti6Sn5 + AuSn2 + AuSn4 + massive Au-Sn-Ti/TiO phase/sapphire.
3. The shear strength of the titanium/AuSn20/Sn-3Ti/sapphire joints first increased and then declined as the temperature increased or the time was prolonged. The highest average strength of 18.7 MPa was obtained for the sample processed at 550 °C for 35 min. The crack started at the sapphire/brazing seam and propagated into the Au-Sn-Ti brittle reactive layer.

Author Contributions: Conceptualization, Y.Z.; investigation, Y.Z.; resources, W.L., S.Z. and L.J.; writing—original draft preparation, Y.Z. and M.S.; writing—review and editing, Y.Z., H.B., X.S. and Y.L.; supervision, H.B., X.S. and Y.L.; project administration, H.B., X.S. and Y.L.; funding acquisition, H.B. and X.S. All authors have read and agreed to the published version of the manuscript.

Funding: This research was funded by the National Natural Science Foundation of China (Grant Nos. 51905127 and 52275321); the Taishan Scholars Foundation of Shandong Province (NO. tsqn201812128); the Innovation Scientists and Technicians Troop Projects of Henan Province (204200510031) and the Heilongjiang Touyan Innovation Team Program (No. HITTY-20190013).

Institutional Review Board Statement: Not applicable.

Informed Consent Statement: Not applicable.

Data Availability Statement: Not applicable.

Acknowledgments: The authors gratefully acknowledge the financial support from the National Natural Science Foundation of China (Grant Nos. 51905127 and 52275321); the Taishan Scholars Foundation of Shandong Province (NO. tsqn201812128); the Innovation Scientists and Technicians Troop Projects of Henan Province (204200510031) and the Heilongjiang Touyan Innovation Team Program (No. HITTY-20190013).

Conflicts of Interest: The authors declare that they have no known competing financial interests or personal relationships that could have appeared to influence the work reported in this paper.

References

1. Mao, W.G.; Shen, Y.G.; Lu, C. Nanoscale elastic-plastic deformation and stress distributions of the C plane of sapphire single crystal during nanoindentation. *J. Eur. Ceram. Soc.* **2011**, *31*, 1865–1871. [CrossRef]
2. Cheng, J.; Wu, J. Experimental investigation of fracture behaviors and subsurface cracks in micro-slot-grinding of monocrystalline sapphire. *J. Mater. Process. Technol.* **2017**, *242*, 160–181. [CrossRef]
3. Guo, W.; Wang, T.; Lin, T.; He, P. Bonding sapphire in air by using Bi_2O_3-B_2O_3 glass braze. *Mater. Lett.* **2018**, *210*, 117–120. [CrossRef]
4. Lee, K.; Gao, Y.; Yao, Z.; Phan, J.; Wu, L.; Liang, J.; Waugh, D.S.; Zhang, Z.; Burke, T.R. Tripeptide inhibitors of Yersinia protein-tyrosine phosphatase. *Bioorg. Med. Chem. Lett.* **2003**, *13*, 2577–2581. [CrossRef]
5. Lin, Z.; Huang, W.; Tsai, J. A study of material removal amount of sapphire wafer in application of chemical mechanical polishing with different polishing pads. *J. Mech. Sci. Technol.* **2012**, *26*, 2353–2364. [CrossRef]
6. Mao, W.G.; Shen, Y.G.; Lu, C. Deformation behavior and mechanical properties of polycrystalline and single crystal alumina during nanoindentation. *Scr. Mater.* **2011**, *65*, 127–130. [CrossRef]
7. Boyer, R.R. An overview on the use of titanium in the aerospace industry. *Mater. Sci. Eng. A* **1996**, *213*, 103–114. [CrossRef]
8. Cui, C.; Hu, B.; Zhao, L.; Liu, S. Titanium alloy production technology, market prospects and industry development. *Mater. Des.* **2011**, *32*, 1684–1691. [CrossRef]

9. Rack, H.J.; Qazi, J.I. Titanium alloys for biomedical applications. *Mater. Sci. Eng. C* **2006**, *26*, 1269–1277. [CrossRef]
10. Siddiqui, M.S.; Jones, W.K. Vacuum Brazing of Alumina to Titanium for Implantable Feedthroughs Using Pure Gold as the Braze Metal. *Int. J. Mater. Sci. Eng.* **2014**, *2*, 56–62. [CrossRef]
11. HU, S.; FENG, D.; XIA, L.; WANG, K.; LIU, R.; XIA, Z.; NIU, H.; SONG, X. Joints of continuous carbon fiber reinforced lithium aluminosilicate glass ceramics matrix composites to Ti60 alloy brazed using Ti-Zr-Ni-Cu active alloy. *Chin. J. Aeronaut.* **2019**, *32*, 715–722. [CrossRef]
12. Dai, X.; Cao, J.; Liu, J.; Wang, D.; Feng, J. Interfacial reaction behavior and mechanical characterization of ZrO_2/TC4 joint brazed by Ag-Cu filler metal. *Mater. Sci. Eng. A* **2015**, *646*, 182–189. [CrossRef]
13. Terasaki, N.; Sakaguchi, M.; Chiba, H.; Ohashi, T.; Nagatomo, Y.; Kuromitsu, Y.; Sekino, T.; Knowles, K.M. Growth mechanism of TiN reaction layers produced on AlN via active metal bonding. *J. Mater. Sci.* **2022**, *57*, 13300–13313. [CrossRef]
14. Wang, Y.; Yang, Z.W.; Zhang, L.X.; Wang, D.P.; Feng, J.C. Low-temperature diffusion brazing of actively metallized Al_2O_3 ceramic tube and 5A05 aluminum alloy. *Mater. Des.* **2015**, *86*, 328–337. [CrossRef]
15. Ghosh, S.; Sengupta, A.; Pal, K.S.; Dandapat, N.; Chakraborty, R.; Datta, S.; Basu, D. Characterization of Metallized Alumina Ceramics. *Metall. Mater. Trans. A Phys. Metall. Mater. Sci.* **2011**, *43*, 912–920. [CrossRef]
16. Hudycz, M. Titanium metallization coating deposited on AlN ceramics substrate by means friction surfacing process. *Weld. Technol. Rev.* **2020**, *92*, 35–44. [CrossRef]
17. Li, J.; Pan, W.; Yuan, Z.; Chen, Y. Titanium metallization of alumina ceramics by molten salt reaction. *Appl. Surf. Sci.* **2008**, *254*, 4584–4590. [CrossRef]
18. Teng, P.; Li, X.; Hua, P.; Liu, H.; Wang, G. Effect of metallization temperature on brazing joints of SiC ceramics and 2219 aluminum alloy. *Int. J. Appl. Ceram. Tec.* **2022**, *19*, 498–507. [CrossRef]
19. Xin, C.; Li, N.; Yan, J. Microstructural evolution in the braze joint of sapphire to Kovar alloy by Ti-Cu metallization layer. *J. Mater. Process. Technol.* **2017**, *248*, 115–122. [CrossRef]
20. Song, X.; Chen, Z.; Hu, S.; Duan, X.; Lei, Y.; Niu, C.; Feng, J. Wetting behavior and brazing of titanium-coated SiC ceramics using Sn0.3Ag0.7Cu filler. *J. Am. Ceram. Soc.* **2020**, *103*, 912–920. [CrossRef]
21. Kang, J.R.; Song, X.G.; Hu, S.P.; Liu, D.; Guo, W.J.; Fu, W.; Cao, J. Wetting and Brazing of Alumina by Sn0.3Ag0.7Cu-Ti Alloy. *Metall. Mater. Trans. A* **2017**, *48*, 5870–5878. [CrossRef]
22. Fu, W.; Passerone, A.; Bian, H.; Hu, S.; Zhao, Y.; Song, X.; Wang, M.; Valenza, F. Wetting and interfacial behavior of Sn-Ti alloys on zirconia. *J. Mater. Sci.* **2019**, *54*, 812–822. [CrossRef]
23. Blugan, G.; Kuebler, J.; Bissig, V.; Janczak-Rusch, J. Brazing of silicon nitride ceramic composite to steel using SiC-particle-reinforced active brazing alloy. *Ceram. Int.* **2007**, *33*, 1033–1039. [CrossRef]
24. Park, J.; Mendez, P.F.; Eagar, T.W. Strain energy release in ceramic-to-metal joints by ductile metal interlayers. *Scr. Mater.* **2005**, *53*, 857–861. [CrossRef]
25. Park, J.; Mendez, P.F.; Eagar, T.W. Strain energy distribution in ceramic-to-metal joints. *Acta Mater.* **2002**, *50*, 883–899. [CrossRef]
26. Zhao, Y.X.; Wang, M.R.; Cao, J.; Song, X.G.; Tang, D.Y.; Feng, J.C. Brazing TC4 alloy to Si_3N_4 ceramic using nano-Si_3N_4 reinforced AgCu composite filler. *Mater. Des.* **2015**, *76*, 40–46. [CrossRef]
27. Li, Q.; Ma, N.; Lei, Y.; Lin, J.; Fu, H.; Gu, J. Characterization of Low-Melting-Point Sn-Bi-In Lead-Free Solders. *J. Electron. Mater.* **2016**, *45*, 5800–5810. [CrossRef]
28. Wang, F.; Wang, H.; Wang, J.; Lu, J.; Luo, P.; Chang, Y.; Ma, X.; Dong, S. Effects of low melting point metals (Ga, In, Sn) on hydrolysis properties of aluminum alloys. *T. Nonferr. Metal. Soc.* **2016**, *26*, 152–159. [CrossRef]
29. Goodman, P. Current and future uses of gold in electronics. *Gold Bull.* **2002**, *35*, 21–26. [CrossRef]
30. Tollefsen, T.A.; Larsson, A.; Løvvik, O.M.; Aasmundtveit, K. Au-Sn SLID Bonding—Properties and Possibilities. *Metall. Mater. Trans. B Process. Metall. Mater. Process. Sci.* **2011**, *43*, 397–405. [CrossRef]
31. Wei, X.; Wang, R.; Peng, C.; Feng, Y.; Zhu, X. Microstructural evolutions of Cu(Ni)/AuSn/Ni joints during reflow. *Prog. Nat. Sci.* **2011**, *21*, 347–354. [CrossRef]
32. Yoon, J.; Chun, H.; Lee, H.; Jung, S. Microstructural evolution and interfacial reactions of fluxless-bonded Au-20Sn/Cu solder joint during reflow and aging. *J. Mater. Res.* **2007**, *22*, 2817–2824. [CrossRef]
33. Yu, D.Q.; Oppermann, H.; Kleff, J.; Hutter, M. Stability of AuSn eutectic solder cap on Au socket during reflow. *J. Mater. Sci. Mater. Electron.* **2009**, *20*, 55–59. [CrossRef]
34. Bobzin, K.; Lugscheider, E.; Ernst, F.; Rösing, J.; Ferrara, S. Challenging gold based filler metals for uses in medicine. *Mater. Sci. Technol.* **2009**, *25*, 1422–1431. [CrossRef]
35. Lei, Y.Z.; Bian, H.; Jang, N.; Song, X.G.; Li, J.C.; Zhao, H.Y.; Long, W.M. Low temperature brazing of biomedical titanium and zirconia metallized with Sn-Ti metal foil. *Mater. Charact.* **2022**, *193*, 112333. [CrossRef]
36. Fu, W.; Song, X.; Passerone, A.; Hu, S.; Bian, H.; Zhao, Y.; Wang, M.; Valenza, F. Interactions, joining and microstructure of Sn-Ti/ZrO_2 system. *J. Eur. Ceram. Soc.* **2019**, *39*, 1525–1531. [CrossRef]
37. Song, X.; Passerone, A.; Fu, W.; Hu, S.; Niu, C.; Zhao, Y.; Wang, M.; Valenza, F. Wetting and spreading behavior of Sn-Ti alloys on SiC. *Materialia* **2018**, *3*, 57–63. [CrossRef]
38. Ali, M.; Knowles, K.M.; Mallinson, P.M.; Fernie, J.A. Interfacial reactions between sapphire and Ag-Cu-Ti-based active braze alloys. *Acta Mater.* **2016**, *103*, 859–869. [CrossRef]

39. Ali, M.; Knowles, K.M.; Mallinson, P.M.; Fernie, J.A. Microstructural evolution and characterisation of interfacial phases in Al_2O_3/Ag-Cu-Ti/Al_2O_3 braze joints. *Acta Mater.* **2015**, *96*, 143–158. [CrossRef]
40. Bian, H.; Liu, Y.; Song, X.; Long, W.; Fu, W.; Chen, Y.; Niu, H. Diffusion bonding of implantable Al_2O_3/Ti-13Nb-13Zr joints: Interfacial microstructure and mechanical properties. *Mater. Charact.* **2022**, *184*, 111665. [CrossRef]
41. Cao, Y.; Yan, J.; Li, N.; Zheng, Y.; Xin, C. Effects of brazing temperature on microstructure and mechanical performance of Al_2O_3/AgCuTi/Fe-Ni-Co brazed joints. *J. Alloy. Compd.* **2015**, *650*, 30–36. [CrossRef]
42. Kar, A.; Mandal, S.; Ghosh, R.N.; Ghosh, T.K.; Ray, A.K. Role of Ti diffusion on the formation of phases in the Al_2O_3-Al_2O_3 brazed interface. *J. Mater. Sci.* **2007**, *42*, 5556–5561. [CrossRef]
43. Laik, A.; Mishra, P.; Bhanumurthy, K.; Kale, G.B.; Kashyap, B.P. Microstructural evolution during reactive brazing of alumina to Inconel 600 using Ag-based alloy. *Acta Mater.* **2013**, *61*, 126–138. [CrossRef]
44. Voytovych, R.; Robaut, F.; Eustathopoulos, N. The relation between wetting and interfacial chemistry in the CuAgTi/alumina system. *Acta Mater.* **2006**, *54*, 2205–2214. [CrossRef]
45. Zhu, W.; Chen, J.; Jiang, C.; Hao, C.; Zhang, J. Effects of Ti thickness on microstructure and mechanical properties of alumina-Kovar joints brazed with Ag-Pd/Ti filler. *Ceram. Int.* **2014**, *40*, 5699–5705. [CrossRef]